Image Cover Sheet

CLASSIFICATION	SYSTEM NUMBER
UNCLASSIFIED	510978

TITLE

MODELING OF HIGH-FREQUENCY SCATTERING FROM ELASTIC SPHERES

System Number:

Patron Number:

Requester:

Notes:

DSIS Use only:

Deliver to:

National Defence
Research and Development Branch

Défense nationale
Bureau de recherche et développement

TECHNICAL MEMORANDUM 98/233
February 1999

MODELLING OF HIGH-FREQUENCY SCATTERING FROM ELASTIC SPHERES

John A. Fawcett

Defence Research Establishment Atlantic

Centre de Recherches pour la Défense Atlantique

Canada

DEFENCE RESEARCH ESTABLISHMENT ATLANTIC

9 GROVE STREET
P.O. BOX 1012
DARTMOUTH, N.S.
CANADA B2Y 3Z7

TELEPHONE: (902) 426-3100
FACSIMILE: (902) 426-9654

CENTRE DE RECHERCHES POUR LA DÉFENSE ATLANTIQUE

9 GROVE STREET
C.P. BOX 1012
DARTMOUTH, N.É.
CANADA B2Y 3Z7

National Defence
Research and Development Branch

Défense nationale
Bureau de recherche et développement

MODELLING OF HIGH-FREQUENCY SCATTERING FROM ELASTIC SPHERES

John A. Fawcett

February 1999

Approved by: R.E. Erickson
Head / Electromagnetics Section

TECHNICAL MEMORANDUM 98/233

Defence Research Establishment Atlantic

Centre de Recherches pour la Défense Atlantique

Canada

Abstract

Acoustic monopoles and the principle of superposition (applied to sound pressure) are fundamental tools that can be used to construct theoretical dipole and cardioid sound sources. Strictly speaking, the size of these monopoles, and their separations when forming simple multipoles like dipole doublets, must be small compared to the wavelengths emitted. In the practical field of sonar transducer design, however, transduction devices have finite dimensions, and consequently, do not meet the basic size and separation criteria for their transmissions to be accurately described by those of multipole sources. Nevertheless, there are transducers that produce good approximations to the omnidirectional, bidirectional, and unidirectional radiation patterns of monopole, dipole, and cardioid sources, respectively. One such device is the low-frequency (900 Hz) directional Class IV flextensional transducer. A single element alone can produce omnidirectional, dipole, and left/right cardioid patterns. This unique capability provides the array designer with many options for generating directional beams, compared to arrays composed solely of omnidirectional sources. In this work, the directivity patterns of a single Class IV element and a four-element orthogonal array are presented. A simple theoretical expression based on multipole sources and the principle of superposition is put forward to qualitatively explain all of the measured patterns. [Work supported in part by the Office of Naval Research]

Résumé

Les monopôles acoustiques et le principe de superposition (appliqué à la pression sonore) sont des outils de base qui peuvent être utilisés pour construire des sources sonores dipôles et cardioïdes théoriques. À strictement parler, la taille de ces monopôles et leurs espacements lorsqu'ils forment des multipôles simples, par exemple des doublets, doivent être petits par comparaison aux longueurs d'onde émises. Cependant, dans le domaine concret de la conception des transducteurs sonars, les dispositifs transducteurs ont des dimensions finies, de sorte qu'ils ne satisfont pas aux critères fondamentaux de taille et d'espacement requis pour que leurs émissions soient décrites avec exactitude par celles des sources multipôles. Néanmoins, il existe des transducteurs qui donnent de bonnes approximations des diagrammes de rayonnement omnidirectionnels, bidirectionnels et unidirectionnels des sources monopôles, dipôles et cardioïdes, respectivement. Mentionnons à titre d'exemple le transducteur flextensionnel directif de classe IV à basse fréquence (900 Hz). Un élément simple peut à lui seul produire des diagrammes omnidirectionnels, dipôles et cardioïdes gauche/droite. Cette capacité unique donne au concepteur de réseaux un grand nombre d'options pour la génération de faisceaux directionnels, comparativement aux réseaux composés uniquement de sources omnidirectionnelles. Dans le présent travail, les diagrammes de directivité d'un élément unique de classe IV et d'un réseau orthogonal à quatre éléments sont décrits. Une expression théorique simple basée sur des sources multipôles et sur le principe de superposition est établie en vue d'expliquer qualitativement tous les diagrammes mesurés. [Travail subventionné en partie par l'Office of Naval Research.]

Executive Summary

Report: DREA Technical Memorandum 98/233
Title: Modelling of high-frequency scattering from elastic spheres
Author: John A. Fawcett
Security Rating: Unclassified

Background:

For sea mine countermeasures applications, high-frequency sonar scattering from an object is usually characterized by a region of higher intensity (highlight region) and a region of low intensity returns (the shadow region). In sidescan sonar image processing, the spatial structure of these highlight/shadow regions are used to classify objects. Often non-mine objects (e.g., boulders) with minelike spatial dimensions can be misclassified as mines. Since every object classified as a potential mine must be investigated further (if there is no historical information on the object) these misclassifications can be very time consuming in a minehunting operation. The signal scattered from an elastic object such as a mine casing may, in fact, contain specular or corner reflections, internal reflections, and energy which travels around the body. These type of features could be used as further classification information and help distinguish mines from seabed clutter. Usually, this type of elastic scattering is studied at frequencies less than 100 kHz, even down to a few kilohertz. In this report we consider the scattering from elastic spheres at frequencies typical of sidescan sonars in order to investigate what classification clues might be present in the resulting backscattered time series.

Principal Results:

It is possible to compute the scattered time series from elastic shelled spheres for the high frequencies typical of sidescan sonars. The simulations show that there is indeed a variation in the details of the backscattered time series as a function of shell thickness and interior fill.

Significance of Results:

These simulations show that at even at the high frequencies typical of sidescan sonars it might be possible to exploit the elastic features in the backscattered time series, in addition to the standard highlight/shadow analysis, to yield better classification performance.

Future Research:

It is hoped that in the future it will be possible to investigate numerically and experimentally the backscattered time series from a variety of mine types and non-mine objects for a range of different frequencies. The use of lower-frequency elastic scattering information in conjunction with higher frequency spatial information could lead to better survey detection/classification capabilities.

INTRODUCTION

Modern active sonars used in mine countermeasures often operate with frequencies of a few-to-several hundred kilohertz. Objects on the seabed or portions of an object, such as rocks, man-made objects or mines, may cause strong sonar returns: the highlight region of the object. This is then followed in the sonar record by a period of very low returns, the so-called shadow region, which is caused by the object blocking the incident sonar signal from reaching the seabed behind.

It is well known that elastic solids or elastic-shelled structures can exhibit a complicated spectral response to an incident wave or, equivalently, in the time domain, the backscattered time series may consist of many different types of arrivals; e.g., (1) specular reflection, (2) circumferential waves, or (3) waves which propagate in the object itself. This means that the highlight region of a target may have additional structure besides the specular reflection and may be significantly extended in time.

In this paper, we consider the simplest of shapes, a sphere, and consider the types of arrivals that might be expected for air-filled spherical elastic shells, water-filled elastic shells, and solid elastic shells for a Gaussian pulse centred at 380 KHz, corresponding approximately to the frequencies used by the MCDV sidescan sonar. We consider qualitatively whether there are any simple clues in the backscattered time series as to which of these three classes of spheres the scatterer belongs. This type of question has been addressed more rigorously in terms of signal processing by, for example, Guanard et al [1] and Abeysekera et al [2]. Kaduchak and Loeffler [3] have recently modelled scattering from various fluid-filled spheres in an investigation of the resultant target strengths and Anson and Chivers [4] have considered high frequency scattering from spherical shells. Our work considers very high frequency scattering - frequencies typical of sidescan sonars - and emphasizes features in the time domain.

I. THEORY

We consider a plane wave incident upon the sphere. In reality, for a sonar system this would be a beam. The theory outlined below can be easily adapted to model a beam shape, both for the source and receiver. We did this in some simulations and found very little difference with the plane wave results. At 380

KHz the wavelength in the water is approximately 4 mm. In this paper we will consider spheres of 0.25 m radius which corresponds to about 60 wavelengths. The theory for the scattering of a plane wave from a spherical shell is well known [1-4]. The unknown compressional and shear potentials are expanded in terms of spherical harmonic functions and a system of equations solved to determine the coefficients of the orders of spherical Hankel and Bessel functions. If one considers an incident plane-wave propagating along the z-axis (and we can always define our coordinate system in free space such that this is true) then we can write the potential for the scattered pressure field in the water in the form

$$\phi_w = \sum_{n=0}^{\infty} a_n h_n(k_w R) P_n(\cos(\theta)) \tag{1}$$

where h_n is the spherical Hankel function of order n, k_w is the wavenumber in water, and R is the three-dimensional distance from the centre of the sphere (the origin) to a point in space. The functions P_n are the Legendre polynomials and θ is the angle measured off the z-axis ($0 < \theta < \pi$). The spherical Hankel functions are chosen for the radial dependance in order that the energy will be "outgoing" at infinity. Within the shell of the sphere there is no such boundary condition on the radial dependance and we write for the compressional potential

$$\phi_{shell} = \sum_{n=0}^{\infty} (b_n h_n(k_{sh}^p R) + c_n j_n(k_{sh}^p)) P_n(\cos(\theta)) \tag{2}$$

and for the shear potential

$$\psi_{shell} = \sum_{n=0}^{\infty} (d_n h_n(k_{sh}^s R) + e_n j_n(k_{sh}^s)) \frac{dP_n(\cos(\theta))}{d\theta} \tag{3}$$

where k_{sh}^p and k_{sh}^s refer to the compressional and shear wavenumbers within the shell respectively. If there is a fluid-filled interior then there would be another series representation for the interior compressional potential; this expansion would involve only the regular spherical Bessel functions j_n as there is the boundary condition that the potential is well-behaved at the origin. The particle displacement, $\vec{u}$, is related to the potentials in the following manner

$$\vec{u} = -\nabla\phi + \nabla \times \psi. \tag{4}$$

From the definition of stresses in terms of particle displacement, the stresses can be expressed in terms of the series expansions above. There are various

continuity conditions of stress and particle displacement which must be satisfied at interfaces and these give rise to equations for the unknown coefficients $(a_n, b_n, c_n, d_n, e_n, f_n)$ in the case of a fluid-filled, shelled sphere. These equations decouple for each value of n. Thus, for an elastic solid there is a 3×3 system to solve, and for a fluid-filled, elastic shell there is 6×6 system to solve for each order n of spherical Hankel and Bessel functions. The known expansion of the incident field is essentially the "right-hand side" of the equations which are solved. The behaviour of the determinant of these equations, as a function of frequency, determines the "resonance " response of the sphere - the occurence of peaks and nulls in the spectral domain. The material properties of the shell, the radius of the sphere and the relative thickness of the shell in terms of the outer radius are important parameters in the study of the scattering of sound from an elastic-shelled sphere.

For an object on the seabed, the incident field will consist of a coherent combination of direct and seabed-reflected energy. Similarly, the downgoing portion of the scattered field from the object will reflect off the seabed and travel back to the receiver, coherently interfering with the direct energy. These interference effects might introduce additional features in the observed backscattered field or in the case that the direct and seabed-reflected pulses overlap with each other, the shape of the pulses in the backscattered signal might be altered (see [5] for some numerical and experimental examples of this for lower frequencies). We will not model the seabed interaction in this paper; the qualtitative conclusions we draw from the free-space cases should also apply to the seabed case, even though the details of the backscattered time series might be different.

For these simulations we are considering the sonar/sphere in a specular geometry. The sphere is a special case for a sonar; a specular direction is guaranteed at some beam angle (or position along a track for a fixed beam direction). For most object shapes this is not the case; a specular reflection will occur only for very specific sonar/object geometries. For more general three-dimensional elastic objects more difficult (and computationally intensive) modelling, such as finite element modelling [6], will have to be used in order to determine whether there are any elastic scattering features which can be exploited for detection or classification purposes.

II. NUMERICAL IMPLEMENTATION

As discussed in Section I, the theory for computing the scattered field for a plane wave incident upon an elastic sphere is well known. There are two features in our numerical code which help us handle the large frequencies (or, in non-dimensional terms large ka values, where k is the wavenumber and a the outer radius of the sphere) used in the computations. First, the value of the spherical Bessel or Hankel function (at one of the radii for the case of a shell) is absorbed into the definition of the functional coefficients. This means that any expression in the system of equations which involves that function, (derivatives, or the value at another radius) will now involve the ratio of functional values (see also [4] for a discussion of the numerical details of high-frequency scattering modelling). Second, the values of the spherical Bessel functions $j_n(x)$ are computed using backwards recursion (the same concept as Miller's algorithm for cylindrical Bessel functions [7]) in the case that $x < n$ and forward recursion otherwise. The spherical functions $y_n(x)$ ($h_n(x) = j_n(x) + iy_n(x)$) are computed using forward recursion; here j_n refer to the regular spherical Bessel functions (spherical Bessel functions of the first kind [8]), y_n refer to spherical Bessel functions which are singular at the origin (spherical Bessel functions of the second kind) and h_n are the spherical Hankel functions, a combination of j_n and y_n which satisfy the outgoing radiation condition at infinity. The values from the recursion schemes are monitored; for $j_n(x)$ the recursion values are renormalized by 10^{-10} if the the values are less than that value and for $y_n(x)$ the values are renormalized by 10^{10} if they exceed that value. By keeping track of the number of times that the recursion series are renormalized, a multiplicative exponential factor is determined for the Bessel function values. These multiplicative factors will often cancel out if they are involved in a subsequent ratio or multiplication. Complex arguments are allowed for in these computations, enabling us to model attenuations. The attenuations are modelled by adding a negative imaginary part to the appropriate sound speed.

In order to illustrate the accuracy of our Bessel function routine we compute the function $j_{400}(x)$ as a function of x. For small values of x compared to ν we can analytically approximate the function by

$$j_\nu(x) \sim \frac{1}{2\sqrt{x(\nu+1/2)}}\left(\frac{ex}{2(\nu+1/2)}\right)^{\nu+1/2}. \tag{5}$$

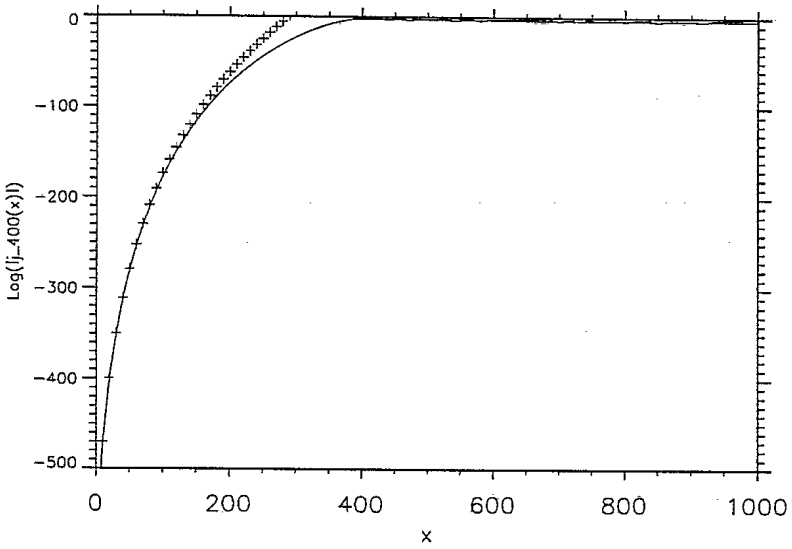

Figure 1: Comparison of asymptotic (small argument expression) (+) and computed spherical Bessel function $log_{10}|j_{400}(x)|$ (solid line)

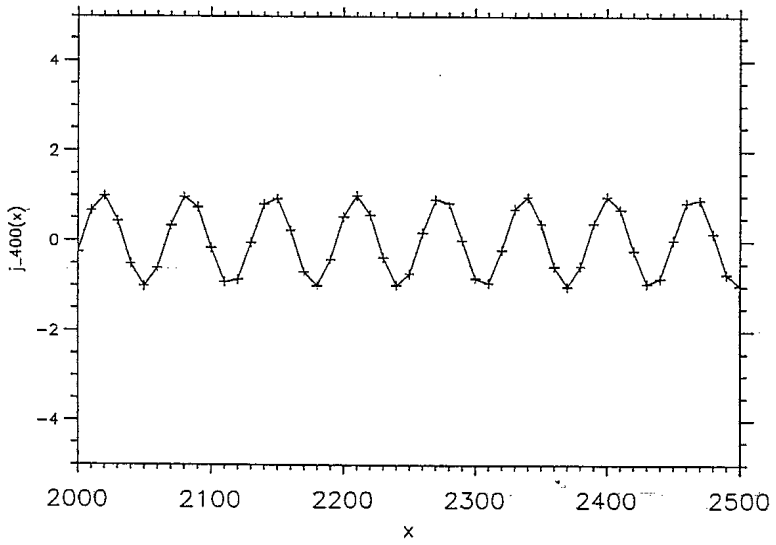

Figure 2: Comparison of asymptotic (large argument expression) (+) and computed spherical Bessel function $xj_{400}(x)$ (solid line)

Similarly for large values of x compared to ν we can use an asymptotic expression [8]

$$j_\nu(x) \sim A(x)\cos(\phi(x)) \tag{6}$$

where

$$A(x) \sim \frac{1}{x}\sqrt{1+\frac{\mu-1}{2(2x)^2}+\frac{3(\mu-1)(\mu-9)}{8(2x)^4}} \tag{7}$$

and

$$\phi(x) \sim x-(\frac{\nu}{2}+\frac{1}{2})\pi+\frac{\mu-1}{8x}+\frac{(\mu-1)(\mu-25)}{6(4x)^3} \tag{8}$$

where $\mu \equiv 4(\nu+1/2)^2$.

As can be seen in Figs.1 and 2 the computed values of this high order spherical function are in excellent agreement with the asymptotic forms of the function for both small and large arguments.

III. NUMERICAL EXAMPLES

We now consider the computed backscattered time series from a series of steel-shelled spheres with air and water fill and a sequence of solid spheres with and without interior attenuation. The solid spheres are chosen to represent very idealized rocks, which by size and shape alone, might be misclassified as a mine. We wish to compare the temporal response of these "rocks" to shelled-structures, both air- and water-filled, which would represent man-made objects. In reality, a mine will have an outer shell and some interior fill such as water, explosives and electronics; it is hoped that the elastic response of such structures might yield some features which would allow them to be distinguished from mine-shaped rocks. For these examples, the incident pulse has the spectral characteristics

$$S(f) = exp(-(f-380000)^2/(2\sigma^2)); \quad \sigma = 30000 \tag{9}$$

This is a tone-burst with a centre frequency of 380 Khz and a bandwidth of 60 kHz from the $-\sigma$ to $+\sigma$ values. The resulting pulse in the time domain is shown in Fig. 3. In order to compute the time-domain scattering solution we compute the harmonic pressure field scattered by the sphere at the frequencies

$$f_i = 333000 + (i-1)*50, \quad i = 1, 2001 \tag{10}$$

and then Fourier synthesize the response using the source weighting of Eq.(5). One slight numerical problem that arises in the time domain is that of wrap-around effects. As we shall see the backscattered time series for many of the

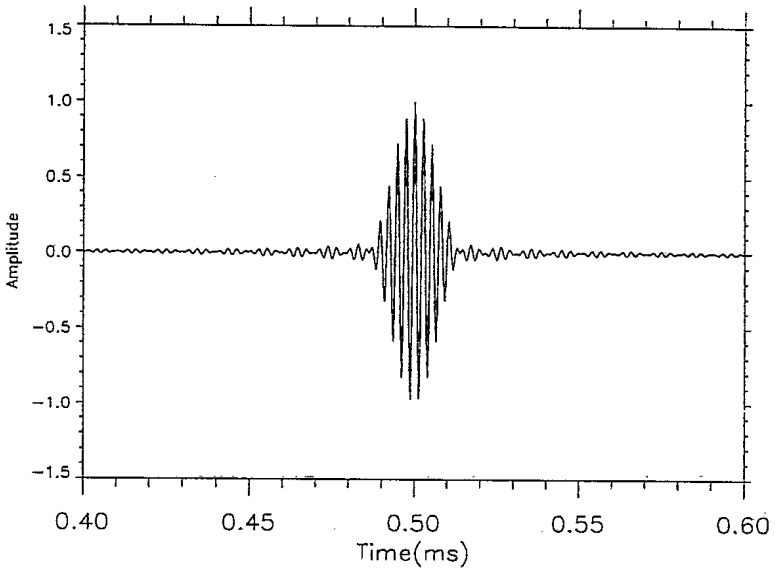

Figure 3: Incident pulse

shells, particularly those with a fluid fill can be extended for several milliseconds. In this case, our Fourier synthesis will yield a small amount of energy in the time domain before the specular reflection - this is non-causal energy and can be regarded as numerical error. There are two ways to reduce this noise: (1) the frequency discretization can be reduced (2) a small amount (e.g. .001 dB/λ) of attenuation can be introduced to the interior fluid.

In the first numerical computations we consider a steel-shell of varying thicknesses (1 mm, 2mm, 4mm and 8 mm). A 1 mm shell might not be realistic to consider for mines, but we have included it for illustrative purposes. For the steel we use the parameters $V_p = 5950$ m/s, $V_s = 3240$ m/s and $\rho = 7700$ kg/m^3. The amplitudes of these time series have been normalized by the maximum amplitude of the incident pulse and multiplied by the range of the receiver, which was set at 20 m for these computations. It is clear from Fig. 4 that besides the specular reflection (the first peak in the time series), there are other significant arrivals in the time series.

The shell of 8 mm thick displays a strong resonance phenomena just behind the specular reflection. This is due to the fact that the compressional wavelength in the shell is $\lambda = 5950/380000 = 15.65$ mm which is almost exactly twice the shell thickness. If higher-frequency pulses were used then this phenomena should

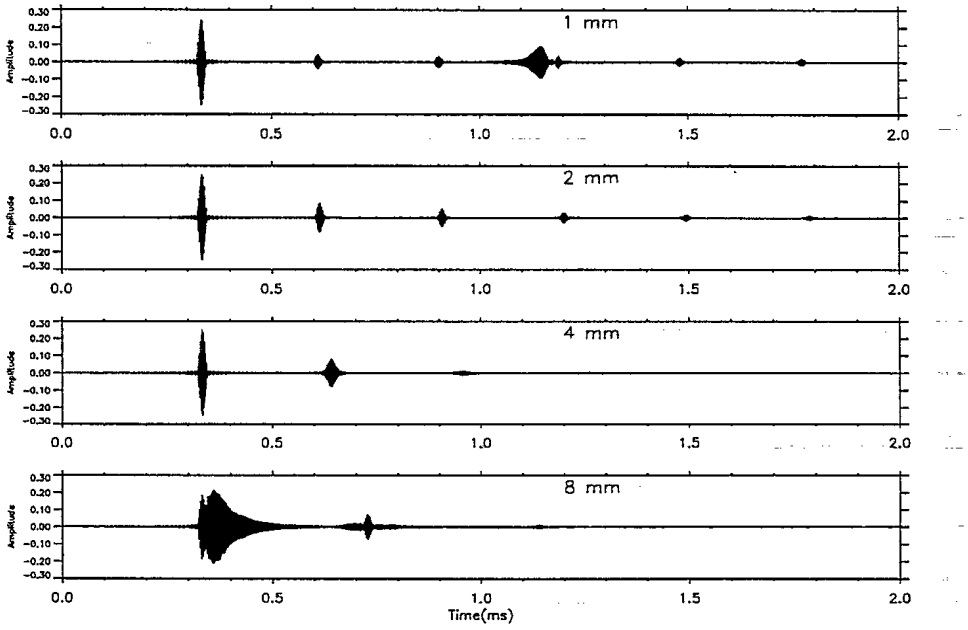

Figure 4: Computed time series as a function of shell thickness (1,2,4, 8 mm) for air interior

occur for smaller shell thicknesses. The other thicknesses are characterized by a dominant specular reflection - which appears as positive reflection (i.e., even for the very thin shells considered the specular reflection is not affected by the air in the interior of the sphere) and a smaller circumferential arrival. For the 1 and 2 mm shells there are a series of equispaced circumferential arrivals. For the 1 mm shell a portion of the spectrum is in the regime near the coincidence frequency (or sometimes called the mid-frequency enhancement region); in this portion of the spectrum the flexural waves [9] make a strong contribution. This wave packet can be observed in the time series of Fig. 4 slightly later than 1.1 ms. Flexural waves are waves with transverse particle motion. Their phase velocity is frequency and shell-thickness dependant. Below the coincidence frequency, their velocity is slower than that of the surrounding water and they do not radiate into the surrounding fluid; at the coincidence frequency their phase velocity is equal to that of the surrounding fluid and they radiate strongly. The study of the types of possible waves which may propagate circumferentially around (and within for a shell with fluid or solid interior) a spherical shell as a function of shell material, shell thickness, and frequency is a complicated subject. On other hand there exist various approximate analytical formulas which relate the travel time of various waves to the shell thickness, and materials. Equivalently, in the spectral domain, the frequencies at which various peaks and nulls occur can also be used to deduce various parameters of the shell, so its is hoped that these elastic phenomena could be used as a valuable classification tool (for example, see [10] for a theoretical and experimental study of the analysis of resonance information from a cylindrical shell).

We now consider the same thicknesses of shell but with a water interior. This now allows for the penetration and propagation of energy in the sphere's interior and gives rise to a much larger variety of possible propagation paths. As can be seen in Fig. 5 the amplitude of the specular reflection is the same as in the air-filled case (please note the scale change for this plot relative to Fig. 4) but now there are other arrivals which are, in fact, stronger in amplitude than the specular energy. Also, the length of time for which the arrivals persist is large; they extend past the time limit of our computation. The two thinnest shells, in particular, have very strong energy arriving just past the 1.1 ms time.

In order to show the temporal extent of the backscattered time series we extend the time window in Fig. 6 below for the 2 mm and 4 mm thick shells. As can be seen, there are arrivals with the same order of magnitude as the

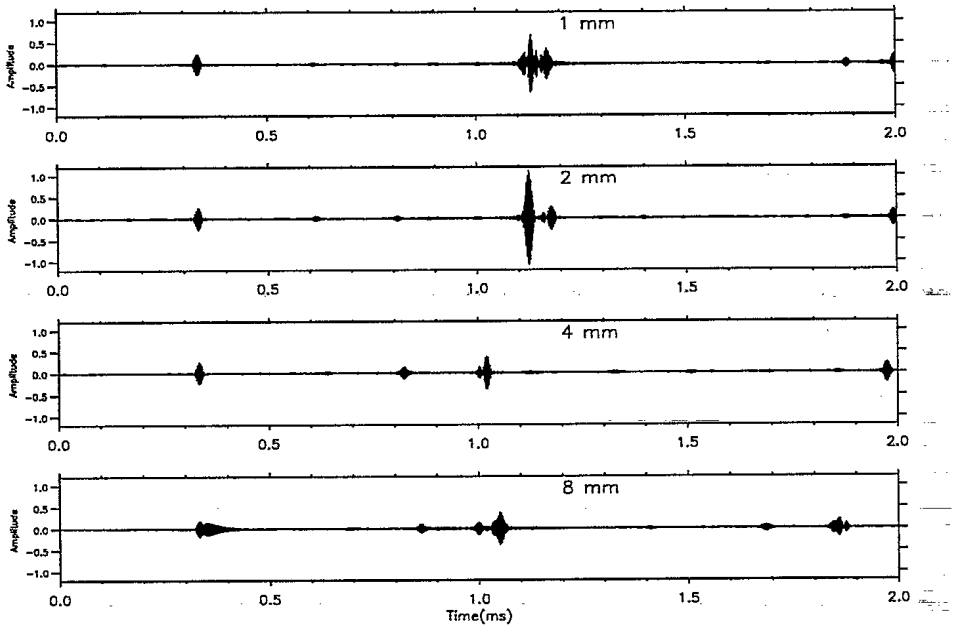

Figure 5: Computed time series as a function of shell thickness (1,2,4, and 8 mm) for water interior - the first peak in the time series is the specular reflection

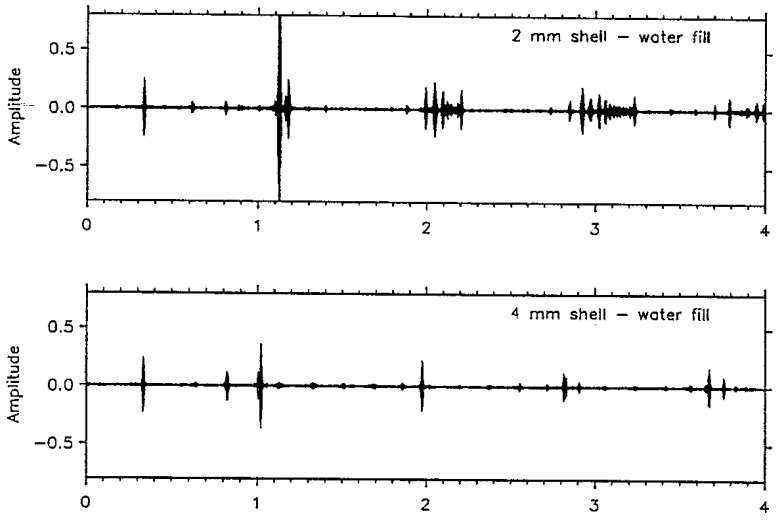

Figure 6: Computed time series as a function of shell thickness (2 and 4 mm) for water interior - extended time window - the first peak is the specular reflection

specular reflection for approximately 2-3 ms. In Fig. 7 the backscattered time series for the air-filled and water-filled shells are directly compared for the 4 mm thick shells. For this figure we used an attenuation of .001 dB/λ for the interior fluid to reduce the amount of temporal wraparound for the water-filled spherical shell. Besides the specular reflection, which appears to be identical for the two types of interior, there is no apparent similarity between the arrival structure of the two time series.

We now consider a sequence of solid objects - "spherical rocks". To give a range of responses, the compressional and shear velocities and the density of the rocks are generated by

$$V_p = 2000\ m/s + (j-1) \times 1250\ m/s; \quad j = 1,4 \tag{11}$$

with

$$V_s = 500\ m/s + (j-1) \times 600\ m/s; \quad j = 1,4 \tag{12}$$

and

$$\rho = 1500 + (j-1) * 400\ g/cm^3; \quad j = 1,4 \tag{13}$$

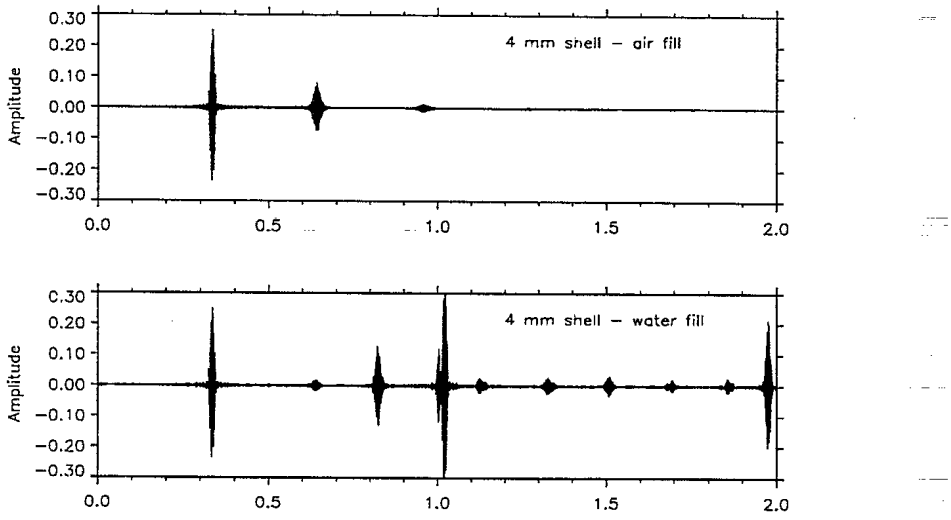

Figure 7: Computed time series for air and water interiors for 4 mm thick steel shell

The resulting time series are shown in Fig. 8. As with the water interior case there are many arrivals, which are stronger than the specular reflection, which arrive later in the time series and these arrivals may persist for a few milliseconds after the specular reflection.

However, in reality rocks have some attenuation; we use 0.1 dB/λ for the compressional wave and 0.2 dB/λ for the shear waves. As one would expect at these high frequencies, the effect of the attenuation is very significant. In Fig. 9 most of the arrival structure, besides the specular reflection, has disappeared; however, some non-specular energy is still evident. In fact, the time series for the 4500 m/s rock is now similar in appearance to that of the 4 mm shell/air results.

The attenuation in steel is relatively very small but at these high frequencies even a small amount may be significant. It is difficult to define a precise value of attenuation for steel as it depends upon precisely what alloy is used and any impurities there might be in the shell. For the results of Fig. 10 use a value of 0.02 dB/λ for the compressional wave and 0.04 dB/λ for the shear wave; Guidarelli et al [11] reported a value of 6.4×10^{-5} Np/mm for a pulse of 951 kHz and a 3 mm plate of steel, which corresponds approximately at this

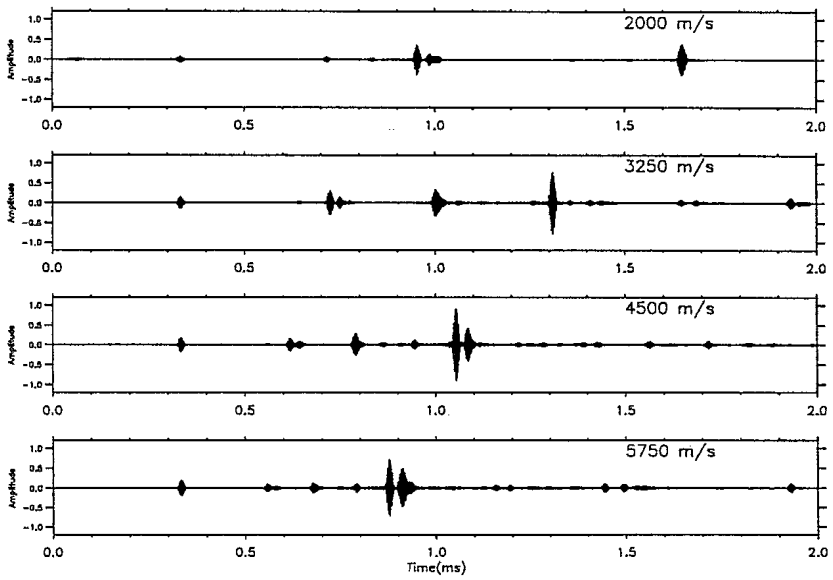

Figure 8: Computed time series as a function of rock type (as denoted by compressional speeds 2000 m/s, 3250 m/s, 4500 m/s, and 5750 m/s)

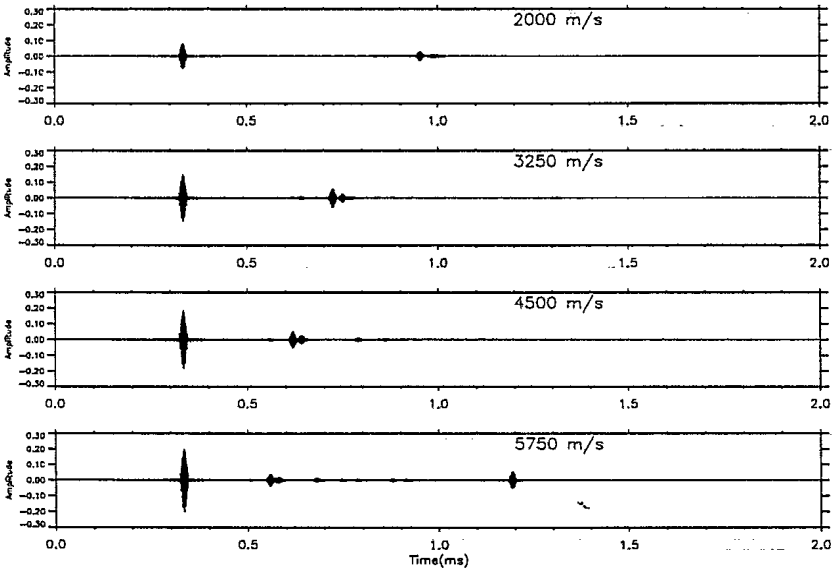

Figure 9: Computed time series as a function of rock type (as denoted by their compressional speed) with attenuation

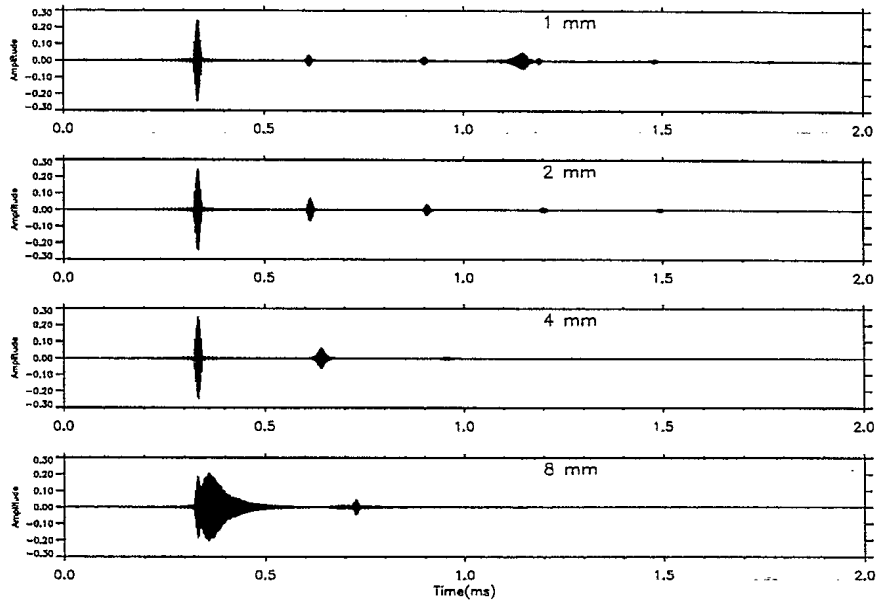

Figure 10: Computed time series as a function of shell thickness (1,2,4 and 8 mm) for air interior with added attenuation

frequency to a compressional attenuation of .003 dB/λ, which is less than we use here in our simulations.

As can be seen the resulting time series are similar to those of Fig. 4 but the later time arrivals have, as one would expect, been diminished somewhat in amplitude. We now repeat these computations in Fig. 11, but for the water-filled shell. In this case, some of the arrivals have been diminished in amplitude while others are essentially unchanged (if fact, one arrival for the 1 mm shell (just after 1.1 ms)is slightly increased in amplitude, probably due to the attenuation of interfering arrivals)

III. SUMMARY

The modelling of scattering of a pulse from a spherical, elastic shell or solid has identified some interesting features. First the specular reflection is positive for even the 1 mm shell thickness. One might expect that for an air-filled shell, that the pulse would be negatively reflected (because of the interior pressure

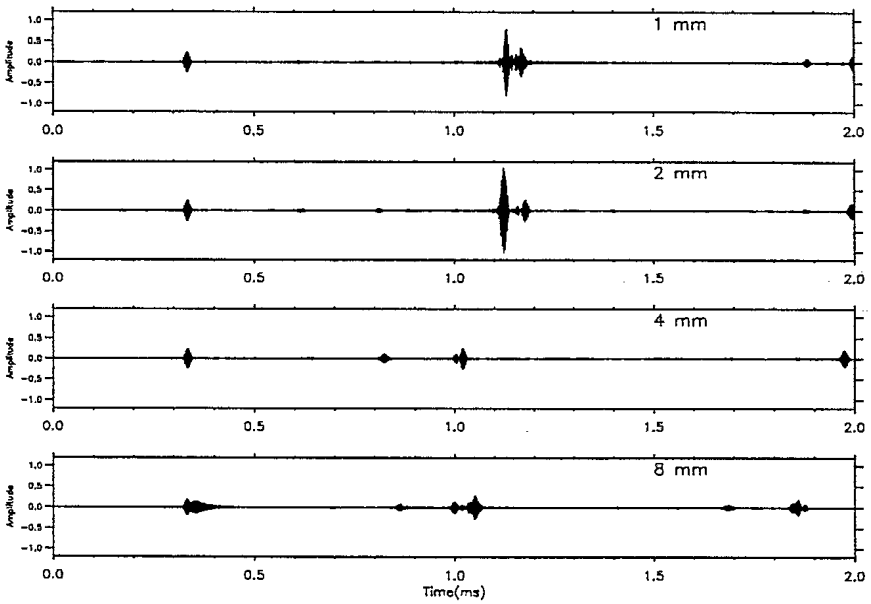

Figure 11: Computed time series as a function of shell thickness for water interior with attenuation in the shell

release boundary). This is, in fact, true for sufficiently thin shells, but for the frequencies considered and the high impedance contrast of the steel, the shells have to be even thinner than 1 mm in order for this to occur. The second main feature is that for all the spheres considered there are always additional arrivals besides the specular reflection. For a steel-shelled air-filled sphere, the specular reflection is dominant and there are then a sequence of circumferential arrivals; for the 4 and 8 mm thick shells there is only one other significant arrival. For the shell of 8 mm there is a strong resonance due to the fact that the shell thickness is a half-wavelength for the centre frequency of the pulse and the steel compressional speed. For the 1 mm thick shell a flexural wave is very evident in the time series.

In the cases of the water-filled sphere and a solid sphere (rock) the later-time arrivals are significantly stronger than the specular reflection and the arrival of energy persists for at least a few milliseconds. However, in the case of the solid spheres the inclusion of a reasonable amount of attenuation for rock types effectively strips away most of these later arrivals. The values of attenuation in metals, used for the shell construction, are often ignored in scattering computations. However, at high frequencies, the attenuations of these materials may be such that they will have a noticeable effect on the computed time series; for the attenuations we used in this paper for the shell, this was not the case, but certainly at higher frequencies the shell attenuation would have a more significant effect. It would be useful to have more precise values for these parameters for modelling purposes.

When attenuation is accounted for, it may prove difficult to simply distinguish the time series from a "fast" spherical rock (e.g, the 4500 m/s rock in our simulations) from a 4 mm steel-shelled, air-filled sphere. However, a fluid-filled sphere should be clearly distinguishable due to its complicated non-specular response, with relatively late, strong arrivals.

The high frequencies used by minehunting sonars are very good in terms of resolving some of the spatial features of an object. The highlight and shadow structure of these sonar images may yield valuable classification information. In this paper, we have shown that the detailed structure of the scattered time series contained within the highlight region might also yield valuable classification information. Although this paper shows that elastic effects of the structure are evident in the time series for the high frequency pulse of minehunting sonars, it would probably be advantageous to consider pulses centred at lower frequencies.

At lower frequencies, the effects of any internal attenuation in an object would be less and scattering from any internal structures might be observed. Also, for many realistic shell thicknesses, lower frequencies (e.g., 40-80 kHz) would contain the coincidence frequency regime for the flexural waves. The results of this paper pertain to spherical shells; it would be useful to model and understand the possible elastic scattering features from more realistic mineshapes and interiors.

References

[1] G.C. Gaunard and H.C. Strifors, "Signal processing of ideal acoustic echoes from submerged shells in the time-frequency domain via Wigner-type distributions," *in Theoretical and Computational Acoustics - Volume I*, edited by J.E. Ffowcs Williams, D.Lee, and A.D. Pierce, World Scientific Publishing Co., 1994.

[2] G. Kaduchak and C. Loeffler, "Relationship between material parameters and target strength of fluid-filled spherical shells in water: calculations and observations" IEEE Journal of Oceanic Engineering, **23**, pp. 26–30 (1998).

[3] S.S. Abeysekara, P.S. Naidu, Y.H. Leung, and H.Lew, "An underwater target classification scheme based on the acoustic backscatter form function, " *in Proceedings of the International Conference on Acoustics, Speech and Signal Processing, ICASSP'98*, pp. 2513-2516.

[4] L.W. Anson and R.C. Chivers, "Ultrasonic scattering from spherical shells including viscous and thermal effects," J. Acoust. Soc. Am., **93**, pp. 1687–1699 (1993).

[5] J.A. Fawcett, W.L.J. Fox and A. Maguer, "Modelling of scattering by objects on the seabed" , to appear in J. Acoust. Soc. Am., 1998

[6] J.A. Fawcett, "Finite element modelling of three-dimensional scattering from azimuthally-symmetric elastic shells," SACLANTCEN Report SR-273, February 1998.

[7] W.H. Press, B.P. Flannery, S.A. Teukolsky, and W.T. Vetterling, *Numerical Recipes in C*, Cambridge Univeristy Press, 1988.

[8] *Handbook of mathematical functions*, editted by M. Abramowitz and I. Stegun, Dover Publications Inc.

[9] R. Lim, J. Lopes, R. Hackman and D. Todoroff, "Scattering by objects buried in underwater sediments: Theory and experiment", J. Acoust. Soc. Am., **93**, pp. 1763–1783, 1993.

[10] A. Tesei, W. Fox, A. Maguer, and A. Lovik, "Resonance scattering analysis by autoregressive models applied to air-filled, cylindrical thin walled shells in water, SACLANTCEN Report SR-265, October 1997.

[11] G. Guidarelli, A. Marini, and L. Palmieri, "Ultrasonic method for determining attenuation coefficients in plate-shaped materials", J. Acoust. Soc. Am., **94**, pp. 1476–1481, 1993.

DOCUMENT CONTROL DATA

(Security classification of title, body of abstract and indexing annotation must be entered when the overall document is classified)

1. ORIGINATOR (the name and address of the organization preparing the document.. Organizations for whom the document was prepared, e.g. Establishment sponsoring a contractor's report, or tasking agency, are entered in section 8.)

Defence Research Establishment Atlantic,
PO Box 1012, Dartmouth,
NS, B2Y 3Z7

2. SECURITY CLASSIFICATION (overall security classification of the document including special warning terms if applicable).

Unclassified

3. TITLE (the complete document title as indicated on the title page. Its classification should be indicated by the appropriate abbreviation (S,C,R or U) in parentheses after the title).

Modelling of high-frequency scattering from elastic spheres (U)

4. AUTHORS (Last name, first name, middle initial. If military, show rank, e.g. Doe, Maj. John E.)

John A. Fawcett

5. DATE OF PUBLICATION (month and year of publication of document)	6a. NO .OF PAGES (total containing information Include Annexes, Appendices, etc).	6b. NO. OF REFS (total cited in document)
February, 1999	(approx.) 22	11

7. DESCRIPTIVE NOTES (the category of the document, e.g. technical report, technical note or memorandum. If appropriate, enter the type of report, e.g. interim, progress, summary, annual or final. Give the inclusive dates when a specific reporting period is covered).

Technical Memorandum

8. SPONSORING ACTIVITY (the name of the department project office or laboratory sponsoring the research and development. Include address).

Defence Research Establishment Atlantic, PO Box 1012, Dartmouth, NS, B2Y 3Z7

9a. PROJECT OR GRANT NO. (if appropriate, the applicable research and development project or grant number under which the document was written. Please specify whether project or grant).	9b. CONTRACT NO. (if appropriate, the applicable number under which the document was written).
Project No. 1da12	

10a ORIGINATOR'S DOCUMENT NUMBER (the official document number by which the document is identified by the originating activity. This number must be unique to this document.)	10b OTHER DOCUMENT NOs. (Any other numbers which may be assigned this document either by the originator or by the sponsor.)
DREA/TM/98/233	

11. DOCUMENT AVAILABILITY (any limitations on further dissemination of the document, other than those imposed by security classification)

(X) Unlimited distribution
( ) Defence departments and defence contractors; further distribution only as approved
( ) Defence departments and Canadian defence contractors; further distribution only as approved
( ) Government departments and agencies; further distribution only as approved
( ) Defence departments; further distribution only as approved
( ) Other (please specify):

12. DOCUMENT ANNOUNCEMENT (any limitation to the bibliographic announcement of this document. This will normally correspond to the Document Availability (11). However, where further distribution (beyond the audience specified in (11) is possible, a wider announcement audience may be selected).

13. ABSTRACT (a brief and factual summary of the document. It may also appear elsewhere in the body of the document itself. It is highly desirable that the abstract of classified documents be unclassified. Each paragraph of the abstract shall begin with an indication of the security classification of the information in the paragraph (unless the document itself is unclassified) represented as (S), (C), (R), or (U). It is not necessary to include here abstracts in both official languages unless the text is bilingual).

Elastic objects, either solid or shelled, may have a complicated temporal response, consisting, possibly of a specular reflection followed by energy which travels circumferentially about the object. As well, energy may propagate and reflect internally within a solid object or fluid-filled shell. Thus, the highlight region of a sonar return may have structure and be extended in time due to the non-specular arrivals.

The elastic responses of spheres, steel-shelled with air or water fill or solid spheres (rocks), are modelled for the high frequencies typical of minehunting sonars and the resulting features in the time domain are examined. The effect of attenuation in the materials is also examined.

14. KEYWORDS, DESCRIPTORS or IDENTIFIERS (technically meaningful terms or short phrases that characterize a document and could be helpful in cataloguing the document. They should be selected so that no security classification is required. Identifiers, such as equipment model designation, trade name, military project code name, geographic location may also be included. If possible keywords should be selected from a published thesaurus. e.g. Thesaurus of Engineering and Scientific Terms (TEST) and that thesaurus-identified. If it not possible to select indexing terms which are Unclassified, the classification of each should be indicated as with the title).

Sonar, spheres, elastic scattering

D
R
E
A

C
R
D
A

#510978